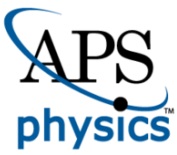

Observation of Nonlinear Standing Waves Excited by Plasma-Series-Resonance-Enhanced Harmonics in Capacitive Discharges

Kai Zhao, De-Qi Wen, Yong-Xin Liu, Michael A. Lieberman, Demetre J. Economou, and You-Nian Wang

Phys. Rev. Lett. **122**, 185002 — Published 7 May 2019

DOI: 10.1103/PhysRevLett.122.185002

Observation of Nonlinear Standing Waves Excited by Plasma Series Resonance-Enhanced Harmonics in Capacitive Discharges

Kai Zhao,[1,2,*] De-Qi Wen,[1,*] Yong-Xin Liu,[1,†] Michael A. Lieberman,[3] Demetre J. Economou,[2] and You-Nian Wang[1,‡]

[1] *Key Laboratory of Materials Modification by Laser, Ion, and Electron Beams (Ministry of Education), School of Physics, Dalian University of Technology, Dalian 116024, China*

[2] *Plasma Processing Laboratory, Department of Chemical and Biomolecular Engineering, University of Houston, Houston, Texas 77204-4004, USA*

[3] *Department of Electrical Engineering, University of California, Berkeley, California 94720, USA*

(Dated: March 20, 2019)

We report the first experimental observation of nonlinear standing waves excited by plasma series resonance-enhanced harmonics in low pressure, very high frequency, parallel plate, capacitively-coupled plasmas. Spatial structures of the harmonics of the magnetic field, measured by a magnetic probe, are in very good agreement with simulations based on a nonlinear electromagnetics model. At relatively low pressure, the nonlinear sheath motion generates high-order harmonics that can be strongly enhanced near the series resonance frequencies. Satisfying certain conditions, such nonlinear harmonics induce radial standing waves, with voltage/current maxima on axis, resulting in center-high plasma density. Excitation of higher harmonics is suppressed at higher pressures.

The sheath dynamics in low pressure capacitively-coupled radio frequency (rf) discharges has long been a central issue of fundamental interest [1–8]. The oscillating sheath plays a dual role: (i) it transfers energy from an external power supply to plasma electrons by collisionless stochastic heating [5–7] and/or electron bounce resonance heating [8], and (ii) it accelerates positive ions from the bulk plasma to a substrate where surface modification takes place. It is also well-recognized that in an asymmetrically excited capacitive discharge, the nonlinear plasma series resonance (PSR) between the capacitive sheath and the inductive bulk plasma drastically enhances electron heating [9, 10]. While the driving frequency is normally below the series resonance frequency, the nonlinear sheath motion generates harmonics that can be strongly enhanced near the series resonance frequencies [11, 12]. Driven at high frequency, these harmonics exist in the form of surface waves that propagate mainly along the sheath-bulk plasma interface. Depending on the gas pressure, the interactions of these surface waves with the plasma can exhibit complex behaviors, e.g., collisional damping due to electron-neutral collisions or collisionless Landau damping due to resonant wave-particle interaction. These harmonic waves, generated by the nonlinear PSR, in turn, significantly influence the local plasma properties (the electron/ion energy distributions) and plasma uniformity. It is, therefore, quite important to understand the fundamentals of the interactions of such harmonics with the plasma.

With the advent of large-area, high-frequency capacitively coupled plasma (CCP) reactors, concerns arise about the plasma non-uniformities, often associated with the standing wave effects (SWE). This phenomenon has been investigated extensively, both by experiment [13–16] and modeling [17–23]. In published studies [13–23], researchers emphasized the role of the fundamental driving frequency. Importantly, nonlinear effects, such as the higher harmonics generated by the PSR, have not received as much attention. Miller *et al.* [24] and Lane *et al.* [25] showed experimentally the existence of harmonic excitations. A correlation between the presence of higher harmonics and center-peaked plasma density profiles was demonstrated by Sawada *et al.* [26]. However, the mechanisms causing these harmonic excitations were not clarified. Lieberman *et al.* and Wen *et al.* brought the coupling of the PSR and SWE into focus [27, 28]. They developed a transmission line model which predicted that the self-excited harmonics by PSR can lead to spatial resonances, significantly enhancing the power deposition in the central region of the reactor. Nevertheless, direct experimental observation of model predictions, such as the spatial structure of the harmonic magnetic field has not yet been reported, to the best of our knowledge.

In this Letter, we report the first experimental evidence of SWE excited by PSR-enhanced harmonics in very high frequency (100 MHz) CCP reactors. Special emphasis is placed on the role of higher harmonic excitations on plasma non-uniformities. To this end, we have employed a high-frequency magnetic probe to determine the radial distribution of the harmonic magnetic field, in combination with a floating double probe to measure the radial distribution of ion (plasma) density. The measured harmonic magnetic field was used to validate a nonlinear electromagnetics model, which in turn was used to uncover the underlying physics.

Experiments were performed in a cylindrical CCP reactor [13, 14], with an inner diameter of 28 cm, containing two stainless steel parallel disk electrodes, 21 cm in diameter, separated by 3 cm. An argon plasma was powered by a 13.56/60/100 MHz sinusoidal voltage ap-

plied to the bottom electrode, while the top electrode and the chamber wall were grounded. The double probe has been described elsewhere [29]. Detailed description of the B-dot probe and validation of the measurements are given in Ref. [30]. To quantitatively determine the harmonic magnetic field strength, the B-dot probe was absolutely calibrated using a Helmholtz coil over the frequency range $2-200$ MHz. The time-domain signal detected by the B-dot probe was transformed into the frequency domain via a fast Fourier transform, giving all harmonics of the magnetic field.

To bring the effect of harmonics into clearer focus, we employed a nonlinear electromagnetic radial transmission line model [27, 28] of a highly asymmetric cylindrical discharge. The discharge was driven at $r = R$ by a voltage source $V_{\rm rf} = V_0 \cos\omega t$ having resistance R_s, through a blocking capacitor C_b. We assumed a cold bulk plasma with a uniform density n_e. The collisionless skin depth δ_p was assumed to be much larger than the plasma thickness d and, the sheath thickness s was assumed to be small compared to the inter-electrode gap l. The experimental CCP reactor was geometrically highly asymmetric, as the effective grounded electrode area was much larger than the powered electrode area. Thus, a dc self-bias $-V_b$ was established on the powered electrode. With a single high voltage sheath (over the powered electrode), radially propagating modes are excited [28],

$$\frac{1}{r}\frac{\partial}{\partial r}\left(r\frac{\partial V_p}{\partial r}\right) = \mu_0 l \frac{\partial J}{\partial t} \tag{1}$$

where V_p is the rf voltage on the powered electrode, μ_0 is the vacuum permeability, and J is the total axial current density. Furthermore, a Neumann boundary at $r = 0$ and Dirichlet boundary at $r = R$ were imposed, respectively.

The current balance equation and the electron momentum balance equation are

$$\frac{\partial \Sigma}{\partial t} = J - J_{i0} + J_{e0} e^{-V_s/T_e}, \Sigma > 0, \tag{2}$$

$$\frac{\partial J}{\partial t} = \frac{e^2 n_e}{md}\left(V_p + V_b - V_s\right) - \nu J, \tag{3}$$

where $\partial\Sigma/\partial t$ is the displacement current, $J_{i0} = e n_e u_B$ is the ion current, $J_{e0} = e n_e v_e/4$ is the electron random thermal current, T_e is the electron temperature, m is the electron mass, and ν is the effective electron collision frequency, with u_B the Bohm speed and v_e the mean electron thermal velocity. A good fit between the time-varying sheath voltage V_s and the time-varying sheath surface charge density Σ for a Child law sheath is $V_s = K\Sigma^{1.681}$, with a Child law factor K as given in Ref. [31].

To shed light on the behavior of higher harmonics, spatially resolved measurements of the harmonic (azimuthal) magnetic field $B_{\varphi,n}$ were performed. Experimentally measured radial distributions of $B_{\varphi,n}$ $(n = 1-5)$ for discharges driven at 13.56 and 100 MHz are shown in Figs. 1(a) and 1(b), respectively. At 13.56 MHz, all harmonics exhibit a similar feature: $B_{\varphi,n}$ is minimum at the center $(r = 0)$ and increases approximately linearly towards the edge $(r = R)$ [Fig. 1(a)]. Assuming azimuthal symmetry and applying Ampere's law, $\mathrm{d}B_{\varphi,n}/\mathrm{d}r$ is proportional to the axial current J_n. The linear increase in $B_{\varphi,n}$ with radius reflects a radially uniform current J_n flowing in the inter-electrode space [Fig. 1(e)]. At 100 MHz, a similar near-linear increase in $B_{\varphi,n}$ vs. radius can be identified for the fundamental frequency $(n = 1)$, shown in Fig. 1(b). For higher harmonics, there is a maximum in $B_{\varphi,n}$ between the center and edge. On the rising edge of $B_{\varphi,n}$, $\mathrm{d}B_{\varphi,n}/\mathrm{d}r$ decreases with radius, corresponding to a substantial reduction of J_n. In other words, the higher-order harmonic currents are mainly concentrated near the center [Fig. 1(f)], which is attributed to the nonlinear standing waves excited by higher harmonics. The measured radial profiles of $B_{\varphi,n}$ are closely reproduced by simulations [Figs. 1(a-b)]. Discrepancies in the absolute magnitude of $B_{\varphi,n}$, shown in Table I, could be due to neglect of external circuit in the model [32] and/or a small difference between the measured voltage and the actual voltage applied on the electrode edge.

Figures 1(c-d) and 1(e-f) show, respectively, simulation results of the radial distributions of the harmonic voltage

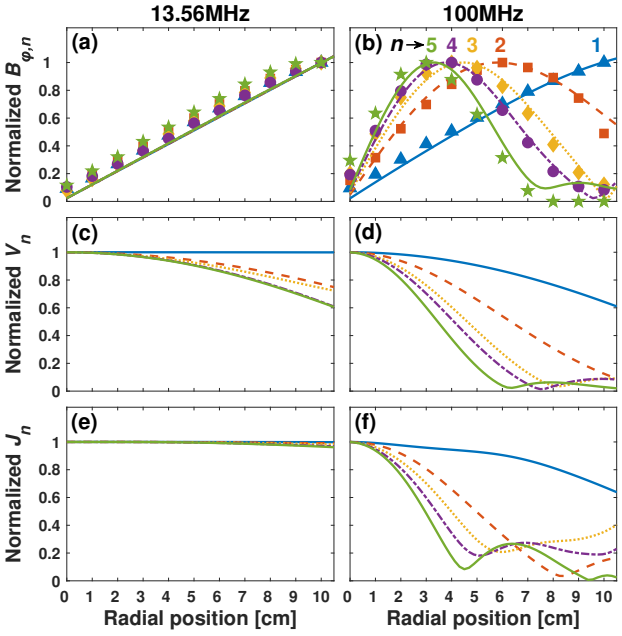

FIG. 1. Experimental data (points) and simulation predictions (lines) for discharges driven at 13.56 MHz (left) and 100 MHz (right) at 3 Pa, for a fixed power of 80 W: radial distributions of the harmonic magnetic field $B_{\varphi,n}$ (a-b), the harmonic voltage V_n (c-d), and the harmonic current J_n (e-f). All harmonic amplitudes $(n = 1-5)$ are normalized to the radial maxima [$B_{\varphi,n,\max}$, $V_{n,\max}$, and $J_{n,\max}$ (see Table I)] to obtain a clearer view of the harmonic structures.

TABLE I. Radial maxima of the physical quantities for the first five harmonics in argon discharges driven at 13.56 and 100 MHz. Other discharge conditions are the same as in Fig. 1.

f [MHz]	13.56					100				
Harmonic order n	1	2	3	4	5	1	2	3	4	5
$B_{\varphi,n,\max}$ (Exp.) [μT]	3.2	0.9	0.5	0.2	0.2	22.8	16.4	-[a]	-[a]	-[a]
$B_{\varphi,n,\max}$ (Sim.) [μT]	2.5	0.8	0.5	0.4	0.3	30.7	10.8	3.2	0.7	0.2
$V_{n,\max}$ (Sim.) [V]	400.8	0.8	0.5	0.5	0.6	94.1	37.6	11.2	3.0	0.7
$J_{n,\max}$ (Sim.) [mA/cm^2]	4.9	1.6	1.0	0.8	0.7	63.5	51.6	19.4	5.1	1.3

[a] Absolute calibration of the B-dot probe at frequencies higher than 200 MHz was limited by the instrumental bandwidth.

V_n and harmonic current J_n. As expected, for the first five harmonics in the 13.56 MHz case, both V_n and J_n exhibit a relatively uniform distribution. Although the radial edge-to-center voltage ratio, $h_V = V_n(R)/V_n(0)$, decreases with n, the resulting plasma density is quite uniform at 13.56 MHz [Fig. 2(a)]. This is because of weak harmonic excitations by PSR (Table I), hence the discharge is actually dominated by the fundamental frequency.

In contrast, the case of 100 MHz is more involved. For $n = 1$, a parabolic-like radial profile of V_n is found [Fig. 1(d)], where the edge-to-center voltage ratio h_V is approximately 0.6, corresponding to a weak SWE. A stronger SWE, with more remarkable center-peaked distribution of V_n ($h_V \approx 0.1$), can be evidently observed for $n = 2$. For $n = 3$, V_n experiences a rapid decline with radius, followed by a moderate rise, going through a valley corresponding to the first node of a standing wave. The distance from the node to the electrode center, R_1, satisfies $k_p R_1 = \chi_{01}$, where $\chi_{01} = 2.405$ is the first zero of the zero-order Bessel function of the first kind, $J_0(\chi)$, and k_p is the wavenumber in the plasma. The wavelength in the plasma $\lambda_p = 2\pi/k_p$ is thus estimated to be about 0.2 m, five times shorter than the vacuum wavelength λ_0. The node position gradually shifts towards the electrode center with increasing n, due to the decreasing wavelength as n increases. Our simulations reveal an abrupt jump in the voltage phase in the vicinity of each node, corresponding to a voltage reversal.

For given n, the distribution of J_n [Fig. 1(f)] resembles that of V_n, but exhibits a shorter distance from the node position to the axis. For $n = 5$, a second node occurs in the inter-electrode space, with the current phase reversing twice as a function of r (see Supplemental Material [30]). The values of $J_{n,\max}$ for different harmonics, shown in Table I, highlight the importance of the first three harmonics, whereas the higher harmonics are less than 10% of the fundamental.

Experimentally measured radial distributions of plasma density for three driving frequencies (13.56, 60, 100 MHz) at 3 Pa are shown in Fig. 2(a). Higher driving frequency yields higher plasma density, due to reduced ion bombardment energies and more efficient electron heating through faster sheath oscillations. More importantly, center-high plasma density non-uniformities are clearly identified with increasing frequency. Results presented thus far demonstrate the important role of higher harmonics (especially the 2nd harmonic), which produce maximum currents on-axis, significantly contributing to the center-high plasma density. In the following, we will analyze the mechanisms causing the plasma non-uniformities based on the spatio-temporal dynamics of the sheath.

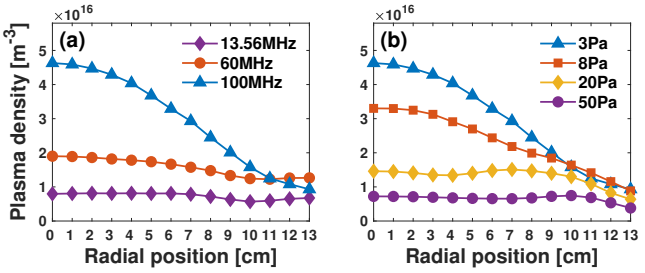

FIG. 2. Measured radial distributions of plasma density in an argon discharge (a) at different driving frequencies (3 Pa, 80 W) and (b) at different pressures (100 MHz, 80 W).

Figures 3(a-b) present simulation results of the sheath thickness s vs. radius in 8 equally-spaced times over one rf cycle at 13.56 and 100 MHz. To elucidate the sheath motion, we also present the corresponding waveforms of the total discharge voltage V and total current density J, at both the electrode center and edge, as shown in Figs. 3(c-d). For both frequencies, stronger current oscillations occur at the center than the edge, as a consequence of the SWE. At 13.56 MHz, the difference in the waveform of J, between the center and edge, mainly lies in the higher harmonics, since only short wavelengths can contribute to the SWE. Due to the fact that the PSR allows a discharge to be sustained with a small voltage, while exhibiting a relatively large current, the difference in the waveform of V is much smaller than that of J. The constancy of the V waveforms as a function of radius leads to nearly identical sheath thickness vs. radius, as illustrated in Fig. 3(a).

In contrast, at 100 MHz, the waveform of V varies distinctly with radius [Fig. 3(d)]. First, the phase of each harmonic wave varies significantly as the surface wave

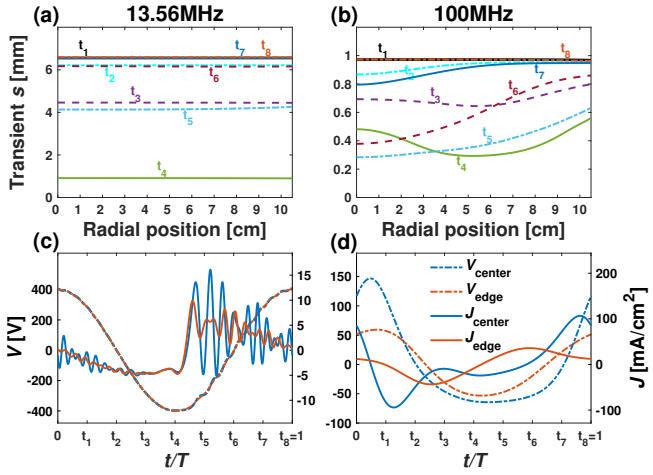

FIG. 3. Simulation results for discharges driven at 13.56 MHz (left) and 100 MHz (right) at 3 Pa, for a fixed power of 80 W: (a) and (b) sheath thickness s vs. radius in 8 equally-spaced times over one rf cycle; (c) and (d) waveforms of the total discharge voltage V (dashed lines) and total current density J (solid lines) at the electrode center ($r = 0$) and edge ($r = R$), over one rf cycle.

propagates from the radial edge to the center. Second, most of the harmonics are enhanced at the center due to significant SWE, resulting in a higher voltage at the center than at the edge. On the other hand, the dc bias on the conductive electrode is constant. Therefore, the sheath collapses to a somewhat smaller thickness at the center than at the edge [Fig. 3(b)]. A higher voltage, a thinner sheath and a higher speed of sheath motion prevail at the center, contributing to a center-high plasma density at 100 MHz, as shown in Fig. 2(a).

The radial non-uniformities in the voltage amplitude, sheath thickness, and plasma density, at 100 MHz, can be interpreted by the nonlinear coupling between the PSR and the spatial wave resonance (SWR). In geometrically asymmetric discharges, PSR will occur between the sheath capacitance $C_s = \epsilon_0/s$ and the bulk plasma inductance $L_p = (l - s)/\epsilon_0(\omega_p{}^2 - \omega^2)$ near the so-called series resonance frequency

$$\omega_{\rm PSR} = \frac{1}{\sqrt{L_p C_s}} = \left(\frac{s}{l}\right)^{1/2} \omega_p, \tag{4}$$

where $\omega_p = (e^2 n_e/\epsilon_0 m)^{1/2}$ is the electron plasma frequency, with ϵ_0 being the vacuum permittivity. Although in general $\omega_{\rm PSR} > \omega$, the expanding/collapsing sheath allows $\omega_{\rm PSR}$ to sweep across multiples of the fundamental frequency, consequently exciting a series of higher harmonics, $N\omega = \omega_{\rm PSR}$ [28].

The wavenumber of radially-propagating surface waves in the discharge is $k = (l/s)^{1/2}\omega_{sw}/c$, where c is the speed of light and ω_{sw} is the wave frequency. Satisfying the condition that the half-wavelength of the surface wave, π/k, becomes comparable to or smaller than the electrode diameter, one can observe a pronounced SWR at

$$\omega_{\rm SWR} = \left(\frac{s}{l}\right)^{1/2} \frac{\chi_{0m} c}{R_m}, \tag{5}$$

where $R_m = \chi_{0m}/k$ is the position of the mth standing-wave node, with χ_{0m} being the mth zero of $J_0(\chi)$. Thus, in the presence of an expanding/collapsing sheath, $\omega_{\rm SWR}$ sweeps across multiples of the fundamental frequency, yielding the excitation of SWR at harmonic frequencies, $M\omega = \omega_{\rm SWR}$. Typically, a strong coupling between the PSR and SWR occurs at $N = M$. Re-inspecting the radial distribution of V_n in Fig. 1 and the harmonic amplitudes in Table I, one notices that in the 100 MHz case, the second-harmonic standing wave excitation is predominant, implying a strong coupling at $N = M = 2$. Interestingly, in the 13.56 MHz case, several weak SWRs induced by the high-order harmonics within the range of $15 < N = M < 29$ were also found (see Supplemental Material [30]).

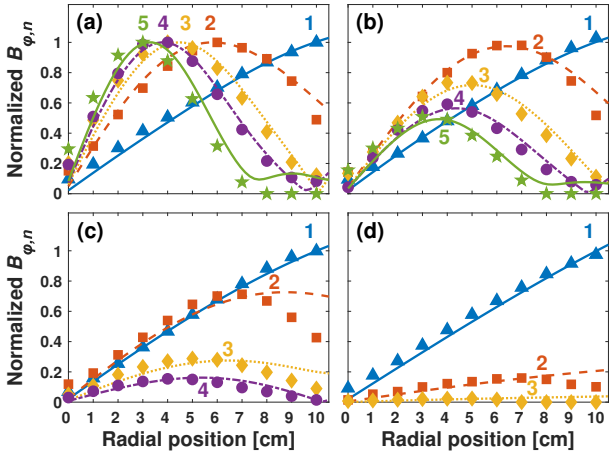

FIG. 4. Experimental data (points) and simulation predictions (lines) of the radial distributions of $B_{\varphi,n}$ at different pressures: (a) 3 Pa, (b) 8 Pa, (c) 20 Pa, and (d) 50 Pa. All harmonic magnetic field amplitudes were normalized to the maxima at 3 Pa. Other conditions were $\omega/2\pi = 100$ MHz, and power = 80 W.

It is not surprising to conclude that the higher harmonics excited by PSR will induce significant SWR under certain conditions. This also implies a positive feedback between PSR and SWR in affecting the plasma uniformity, i.e., the center-high fundamental-frequency voltage dominated by SWR allows the oscillating sheath boundary to traverse a larger distance at the electrode center, which in turn generates higher harmonics [Eq. (4)], enhancing the voltage on-axis, leading to worse plasma non-uniformities. This sequence can be, nevertheless, interrupted by increasing gas pressure. Measured radial distributions of harmonic magnetic field strength at different pressures ($3 - 50$ Pa) are shown in Fig. 4. Again a good agreement between experiment and simulation is seen.

The higher harmonics decay dramatically with pressure, resulting in improved plasma uniformity [Fig. 2(b)]. At higher pressures, the SWE at the fundamental frequency is damped, due to more frequent electron momentum transfer collision with the background gas, giving rise to a weaker initial excitation of nonlinear harmonics. This, combined with a temporally faster decay at higher pressures [27], primarily explains the suppression of higher harmonics with increasing pressure (Fig. 4), which also yields lower plasma density [Fig. 2(b)].

In conclusion, we investigated the nonlinear standing waves excited by plasma series resonance (PSR) in very high frequency (100 MHz) CCP reactors. At low pressure, higher harmonics enhanced by PSR were found to induce spatial wave resonances (SWRs), with voltage/current peaked on-axis, leading to center-high plasma density. Specifically, the dominant role of the second harmonic on the plasma non-uniformity was demonstrated. Standing waves at higher harmonics ($n = 3 - 5$) were also present, but were much weaker compared to the second harmonic. Excitation of the higher harmonics was suppressed at higher pressures, resulting in improved plasma uniformity. The interactions of the high-order harmonics with the plasma are not only of fundamental importance, but also practically meaningful for optimizing the plasma uniformity towards the next generation of 450 mm plasma processing systems in the semiconductor industry.

This work was supported by the National Natural Science Foundation of China (NSFC) (Grant Nos. 11335004 and 11722541). MAL acknowledges the partial support of the Department of Energy Office of Fusion Energy Sciences (Contract No. DE-SC0001939). DJE is grateful to the National Science Foundation (Grant No. PHY-1500518) and to the Department of Energy Office of Fusion Energy Science (Contract No. DE-SC0001939) for financial support.

* These authors contributed equally to this work.
† yxliu129@dlut.edu.cn
‡ ynwang@dlut.edu.cn

[1] G. Y. Park, S. J. You, F. Iza, and J. K. Lee, Phys. Rev. Lett. **98**, 085003 (2007).
[2] I. D. Kaganovich, Phys. Rev. Lett. **89**, 265006 (2002).
[3] J. Schulze, A. Derzsi, K. Dittmann, T. Hemke, J. Meichsner, and Z. Donko, Phys. Rev. Lett. **107**, 275001 (2011).
[4] M. M. Turner, Phys. Rev. Lett. **75**, 1312 (1995).
[5] G. Gozadinos, M. M. Turner, and D. Vender, Phys. Rev. Lett. **87**, 135004 (2001).
[6] M. M. Turner and P. Chabert, Phys. Rev. Lett. **96**, 205001 (2006).
[7] J. Schulze, B. G. Heil, D. Luggenhölscher, R. P. Brinkmann, and U. Czarnetzki, J. Phys. D: Appl. Phys. **41**, 195212 (2008).
[8] Y. X. Liu, Q. Z. Zhang, W. Jiang, L. J. Hou, X. Z. Jiang, W. Q. Lu, and Y. N. Wang, Phys. Rev. Lett. **107**, 055002 (2011).
[9] T. Mussenbrock, R. P. Brinkmann, M. A. Lieberman, A. J. Lichtenberg, and E. Kawamura, Phys. Rev. Lett. **101**, 085004 (2008).
[10] U. Czarnetzki, T. Mussenbrock, and R. P. Brinkmann, Phys. Plasmas **13**, 123503 (2006).
[11] M. Klick, J. Appl. Phys. **79**, 3445 (1996).
[12] B. P. Wood, M. A. Lieberman, and A. J. Lichtenberg, IEEE Trans. Plasma Sci. **19**, 619 (1991).
[13] Y. X. Liu, Y. S. Liang, D. Q. Wen, Z. H. Bi, and Y. N. Wang, Plasma Sources Sci. Technol. **24**, 025013 (2015).
[14] K. Zhao, Y. X. Liu, E. Kawamura, D. Q. Wen, M. A. Lieberman, and Y. N. Wang, Plasma Sources Sci. Technol. **27**, 055017 (2018).
[15] G. A. Hebner, E. V. Barnat, P. A. Miller, A. M. Paterson, and J. P. Holland, Plasma Sources Sci. Technol. **15**, 879 (2006).
[16] A. Perret, P. Chabert, J. Jolly, and J. P. Booth, Appl. Phys. Lett. **86**, 021501 (2005).
[17] L. Sansonnens, A. A. Howling, and C. Hollenstein, Plasma Sources Sci. Technol. **15**, 302 (2006).
[18] E. Kawamura, M. A. Lieberman, and D. B. Graves, Plasma Sources Sci. Technol. **23**, 064003 (2014).
[19] I. Lee, D. B. Graves, and M. A. Lieberman, Plasma Sources Sci. Technol. **17**, 015018 (2008).
[20] P. Chabert, J. L. Raimbault, J. M. Rax, and M. A. Lieberman, Phys. Plasmas **11**, 1775 (2004).
[21] S. Rauf, K. Bera, and K. Collins, Plasma Sources Sci. Technol. **17**, 035003 (2008).
[22] D. Eremin, T. Hemke, R. P. Brinkmann, and T. Mussenbrock, J. Phys. D: Appl. Phys. **46**, 084017 (2013).
[23] M. Lieberman, J. Booth, P. Chabert, J. Rax, and M. Turner, Plasma Sources Sci. Technol. **11**, 283 (2002).
[24] P. A. Miller, E. V. Barnat, G. A. Hebner, A. M. Paterson, and J. P. Holland, Plasma Sources Sci. Technol. **15**, 889 (2006).
[25] B. Lane, C. Campbell, I. Sawada, and P. L. G. Ventzek, J. Vac Sci. Technol. A **34**, 031302 (2016).
[26] I. Sawada, P. L. G. Ventzek, B. Lane, T. Ohshita, R. R. Upadhyay, and L. L. Raja, Japan. J. Appl. Phys. **53**, 03DB01 (2014).
[27] D. Q. Wen, E. Kawamura, M. A. Lieberman, A. J. Lichtenberg, and Y. N. Wang, Plasma Sources Sci. Technol. **26**, 015007 (2016).
[28] M. A. Lieberman, A. J. Lichtenberg, E. Kawamura, and A. M. Marakhtanov, Plasma Sources Sci. Technol. **24**, 055011 (2015).
[29] X. Z. Jiang, Y. X. Liu, S. Yang, W. Q. Lu, Z. H. Bi, X. S. Li, and Y. N. Wang, J. Vac Sci. Technol. A **35**, 011006 (2011).
[30] See Supplemental Material for details.
[31] D. Q. Wen, E. Kawamura, M. A. Lieberman, A. J. Lichtenberg, and Y. N. Wang, Phys. Plasmas **24**, 083517 (2017)
[32] Y. Yamazawa, Appl. Phys. Lett. **95**, 191504 (2009).